Climate Dynamics (2021) 56:1937–1949
https://doi.org/10.1007/s00382-020-05568-w

Subtropical modulation of the equatorial undercurrent: a mechanism of Pacific variability

Lauren B. Kuntz[1] · **Daniel P. Schrag**[1]

Received: 22 December 2019 / Accepted: 2 December 2020 / Published online: 4 January 2021

Abstract
Combining data from Argo and the TAO buoy array we present new observations of variability in the Pacific Ocean. Argo profiles reveal the development of a thickness anomaly in the lower levels of the ventilated thermocline of the South Pacific in 2010. Data through 2017 show this anomaly propagating as a baroclinic wave westward and towards the equator. Theory suggests that this wave will reduce the velocity of the equatorial undercurrent (EUC) when it reaches the equator, transitioning the equatorial Pacific to a warm state. This is supported by TAO array observations that show a past decadal shift in EUC strength around 2000, as well as radiocarbon coral measurements which suggest a similar change in the 1970s, both of which align with phase changes in Pacific decadal variability. Using model simulations with enhanced vertical resolution in the thermocline, we affirm this link between the subtropical south Pacific thermocline and the EUC, which also manifests in eastern Pacific sea surface temperatures. We combine these results to hypothesize a mechanism that may explain some of the decadal variability observed in the Pacific. This mechanism relies on the propagation of anomalies in the structure of the ventilated thermocline from the southeastern Pacific to the equatorial Pacific, modulating the strength of the EUC. The cycle is enhanced by atmospheric teleconnections between the equatorial Pacific and the southeast Pacific that periodically reverse the anomaly in thermocline thickness. If correct, our hypothesis predicts a return to a warm state of the equatorial Pacific when the Kelvin wave reaches the equator and the thermocline adjustment slows the EUC.

1 Introduction

Multi-decadal variability in the Pacific Ocean is dominated by the Pacific Decadal Oscillation (PDO), defined by a pattern of sea surface temperature (SST) variations in the North Pacific. The PDO has a spatial signature throughout the Pacific basin that resembles El Niño Southern Oscillation (ENSO), and has been tied to climate, ecological, and socio-economic impacts around the world (Trenberth and Hurrell 1994; Mantua and Hare 2002). Based on the similar spatial footprint between the PDO and ENSO, some studies hypothesized that the PDO was simply a decadal manifestation of ENSO, with no specific physical mechanism (Barsugli and Battisti 1998; Newman et al. 2003). An alternative view attributes the PDO to a combination of physical processes acting on different timescales and in different locations (Newman et al. 2016).

Circulation in the ventilated thermocline of the tropical Pacific, which links waters subducted in the subtropics to those upwelling in the tropics, has been a focus of many studies that discussed possible mechanisms for the PDO and low-frequency variability in the equatorial Pacific. The linkage between the subtropics and tropics through the ventilated thermocline was supported by the distribution of bomb radiocarbon (e.g., Broecker et al. 1985, 1995) as well as the penetration of a subtropical tritium signal into the Eastern Pacific (Fine et al. 1987). The delayed radiocarbon signal in corals (e.g., Druffel 1987) also pointed to a ventilated thermocline circulation with a multi-decadal timescale. A number of ideas have suggested that variability along this circulation pathway could generate decadal variability throughout the Pacific basin. Advection of temperature anomalies (Gu and Philander 1997; Bratcher and Giese 2002; Giese et al. 2002), shifts in the contribution of waters from the northern and southern hemisphere (Guilderson and Schrag 1998;

Supplementary Information The online version contains supplementary material available at https://doi.org/10.1007/s00382-020-05568-w.

✉ Lauren B. Kuntz
lkuntz2013@gmail.com

[1] Department of Earth and Planetary Sciences, Harvard University, Cambridge, MA, USA

Rodgers et al. 1999), and anomalous water transport (Kleeman et al. 1999) have all been proposed as physical mechanisms for PDO variability. Focusing on low-frequency variability in the equatorial Pacific, as opposed to exclusively PDO signals, Jin (2001) used linear shallow-water theory to suggest an ENSO-like recharge-discharge oscillation linked to subtropical Rossby waves via thermocline perturbations. However, direct observation of any such thermocline anomalies remains elusive. Analysis of subsurface temperatures in both the North Pacific (Schneider et al. 1999a, b; Hazeleger et al. 2001) and South Pacific (Kolodziejczyk and Gaillard 2012) failed to find coherent propagation of temperature anomalies within the ventilated thermocline. With Argo data from 2004 to 2017, we performed an analysis of subsurface thermocline temperatures that also fails to show coherent propagation of temperature anomalies in both the North and South Pacific (Fig. S1, S2), calling to question its link to the PDO.

Here, we present a series of new observations and build upon a series of earlier studies that explore wave propagation as a mechanism for decadal variability in the tropical Pacific (Godfrey 1975; Lysne et al. 1997; Jin 2001). Initial theoretical work by Godfrey (1975) demonstrated the ability of subtropical thermal anomalies to propagate via a progression of waves to the equator. Lysne et al. (1997) furthered those ideas using numerical models and observations to suggest a wave mechanism operating in the North Pacific that impacts low-frequency equatorial variability. Using theoretical arguments, Jin's (2001) work solidified the wave mechanism dynamics at play which can modulate the state of the Pacific on decadal timescales: planetary-scale baroclinic waves in the mid-latitudes can modify the density structure of the equator, coupling with SSTs and wind stress. Here we provide observational evidence of such waves propagating from the subtropical South Pacific. We expand upon these previous ideas, linking the resulting modifications of the thermocline density structure to sustained shifts in the average velocity of eastward-moving cold water in the equatorial undercurrent (EUC). We use observations, simplified analytical theory of ventilated thermocline transport, and model simulations, to explore this mechanism.

2 Data and methods

2.1 Observational datasets

Using the Roemmich-Gilson Argo Climatology (Roemmich and Gilson 2009, 2018), we track heat content, thickness, and temperature anomalies along the ventilated thermocline. We use monthly averages of temperature and salinity to calculate potential density with depth. We interpolate the temperature and pressure data onto potential density anomaly coordinates with 13 levels between 25 and 27 σ_θ (kg m^{-3}). As the interpolation can only be performed if potential density is increasing with depth, we remove any density inversions by modifying the density profile to maintain a monotonic increase with depth. This allows us to calculate heat content, thickness, and average temperature between 25.5 and 26.5 σ_θ—the range of density value composition within the equatorial undercurrent that feeds the upwelling region in the eastern tropical Pacific (Rodgers et al. 2003). We take the 1-year running mean to low-pass filter the data and then subtract the 2004 mean from the record to consider anomalies relative to the start of the Argo observational period.

We use current measurements from the equatorial buoy in the Tropical Atmosphere Ocean (TAO) array at 140°W (and 110°W in the Supplement) to explore the variability in EUC transport strength (TAO Project Office 2000). We primarily use data from the acoustic doppler current profilers (ADCP), but fill in missing data with the current meters. To create a smooth profile and fill in any measurement gaps with depth, we perform a piecewise cubic interpolation on the monthly data, calculating velocity every 5 m. To look at the EUC transport, we define the core of the undercurrent to be the region with speeds greater than 80 cm/s. We calculate the depth-integrated velocity over that region for months with observations. We discard the fluxes from a given month if the velocity of the bottommost measurement exceeds 80 cm/s. As some of the velocity profiles do not cover the full depth range over which zonal velocity is positive, this removes the possibility that the buoy only sampled part of the EUC for that month. Prior to averaging data, we remove the seasonal cycle to avoid biasing the average due to months with missing data. We do not include the 1997/1998 El Nino and following La Nina in the calculation of the seasonal cycle.

2.2 Reanalysis data

Corresponding with the period of Argo observations (2004—present), we use monthly mean wind stress from the ERA-Interim reanalysis (Dee et al. 2011) to examine circulation patterns that could explain changes in the ventilated thermocline. We look at anomalies in the annual average as well as anomalies in southern Hemisphere winter (July, August, September) to reflect the period of maximum subduction in the South Pacific. For consistency with the Argo analysis and to allow for direct comparison, we take anomalies relative to 2004.

2.3 Model simulations

We run the National Center for Atmospheric Research's Community Earth System Model (CESM) with pre-industrial conditions and various forcings. The simulations are

performed on a 1-degree ocean grid and 2-degree atmospheric grid, with the Community Atmosphere Model version 4.0 (CAM4) coupled to the Parallel Ocean Program version 2 (POP2). The meridional resolution of the ocean model increases to roughly 1/3-degree near the equator (Hurrell et al. 2013). This telescoping resolves the equatorial Rossby radius (about 290 km), enabling the resolution of equatorial Kelvin waves and the equatorial undercurrent in the meridional direction (Ng and Hsieh 1994).

We explore the impact of off-equatorial changes in the thermocline structure on the equatorial circulation. The vertical resolution of the ocean model in CESM is increased from 60 to 70 layers by modifying the top 400 m such that the grid spacing is 10 m. Control and perturbation cases are run for 50 and 20 years respectively. In the two perturbation cases, the salinity profiles are adjusted between 30 to 40°S and 135°E to 150°W to either shoal or deepen the 26.5 σ_θ surface. The depths of the 25.5 and 27 σ_θ levels are held constant, but the 26.5 level is shoaled (depressed), doubling the distance to the 27 σ_θ surface (cutting the distance to the 27 σ_θ surface in half). These perturbations are achieved by modifying salinity such that potential density increases piecewise linearly with depth from the new 26.5 σ_θ level up to 25.5 σ_θ and down to 27 σ_θ. To maintain the isopycnal thickness anomaly, both temperature and salinity profiles are restored in this region over the course of the simulation with a restoring timescale of 20 days. The restoring timescale increases outside this region over roughly 1.5 degrees latitude and 5.5 degrees longitude. For both simulations (control and perturbation cases) we calculate the Nino3.4 region (5° S–5° N, 120–170 °W) SSTs, and the vertically integrated EUC flow rate at 140° W. We also calculate the PDO index for both simulations as well as the Interdecadal Pacific Oscillation (IPO) index, which is similar to the PDO but is based on SST variability in the eastern equatorial Pacific, instead of the North Pacific. We define the model IPO and PDO as the leading area-weighted EOF pattern of SST anomalies in the Pacific and North Pacific respectively, after removing the seasonal cycle of the control simulation. We use these patterns to calculate the IPO and PDO time series in the perturbation simulations.

We also perform an additional perturbation case, where a deepening anomaly is applied just off the equator in the western Pacific between 5 to 10° S and 135° E to 150° W. As before, we hold the depths of the 25.5 and 27 σ_θ levels constant and depress the 26.5 level by cutting the distance to the 27 σ_θ surface in half. The perturbation is maintained throughout the simulation as described above. To diagnose the impact of the thermocline perturbation on equatorial circulation, we look at the equatorial response at 140 °W in terms of both zonal velocity and potential density to this perturbation. We perform this analysis on the two mid-latitude perturbations as well.

3 Observational results

3.1 Ventilated thermocline and wind stress anomalies

Figure 1 shows a sequence of maps of isopycnal thickness changes from 2006 to 2017 in the South Pacific between 25.5 and 26.5 σ_θ—the range of isopycnal composition within the equatorial undercurrent that feeds the upwelling region in the eastern tropical Pacific (Rodgers et al. 2003). Between 2009 and 2012, a thickening of the isopycnal layers develops in the subtropical central South Pacific and subsequently propagates as a planetary-scale first-baroclinic mode wave. The observed increase in layer thickness of roughly 50 m reflects a 25% increase in the baseline layer thickness. This increase in isopycnal layer thickness corresponds with an increase in heat content (Fig. S3), but does not correspond with temperature changes (Fig. S2). A different visualization that supports the identification of Rossby wave propagation is a Hovmoller diagram that shows the depth of the base of the thermocline (26.5 σ_θ) between 25 and 40°S in the Pacific (Fig. 2). As in Chelton and Schlax (1996) and Chelton et al. (2007), altimeter data could be used to strengthen the identification of baroclinic Rossby wave propagation. A preliminary review of this data shows some indication of this wave (Fig. S5). Observations of sea level from the Copernicus Marine Environment Monitoring Service gridded product (von Schuckmann et al. 2016) reveal anomalies developing and propagating from a similar region, but the anomalies are not as clear as with the isopycnal thickness. These could be due to additional waves captured in the sea level signal as well as long-term trends; further analysis is a worthwhile endeavor. We observe no similar change in the North Pacific (Fig. S6). Thickening of isopycnal layers does occur in the North Pacific, but appears to dissipate quickly and does not propagate as a baroclinic wave.

Over the same period, reanalysis data reveal a strengthening of the positive wind stress curl during Southern Hemisphere winter (Fig. S7). Particularly during 2010 and 2011, when the baroclinic wave is formed, there is a positive, sustained anomaly in the annual average wind stress curl in the southern subtropics (Fig. S8). This wind stress anomaly should increase Ekman pumping causing net convergence and downwelling in the subduction zone of the ventilated thermocline (Rodgers et al. 2003), possibly explaining the development of the thermocline thickness anomaly.

3.2 Changes in the equatorial undercurrent

Figure 3 shows the EUC velocity from the TAO buoys at 140° W. Around 2000, the EUC accelerates, particularly at

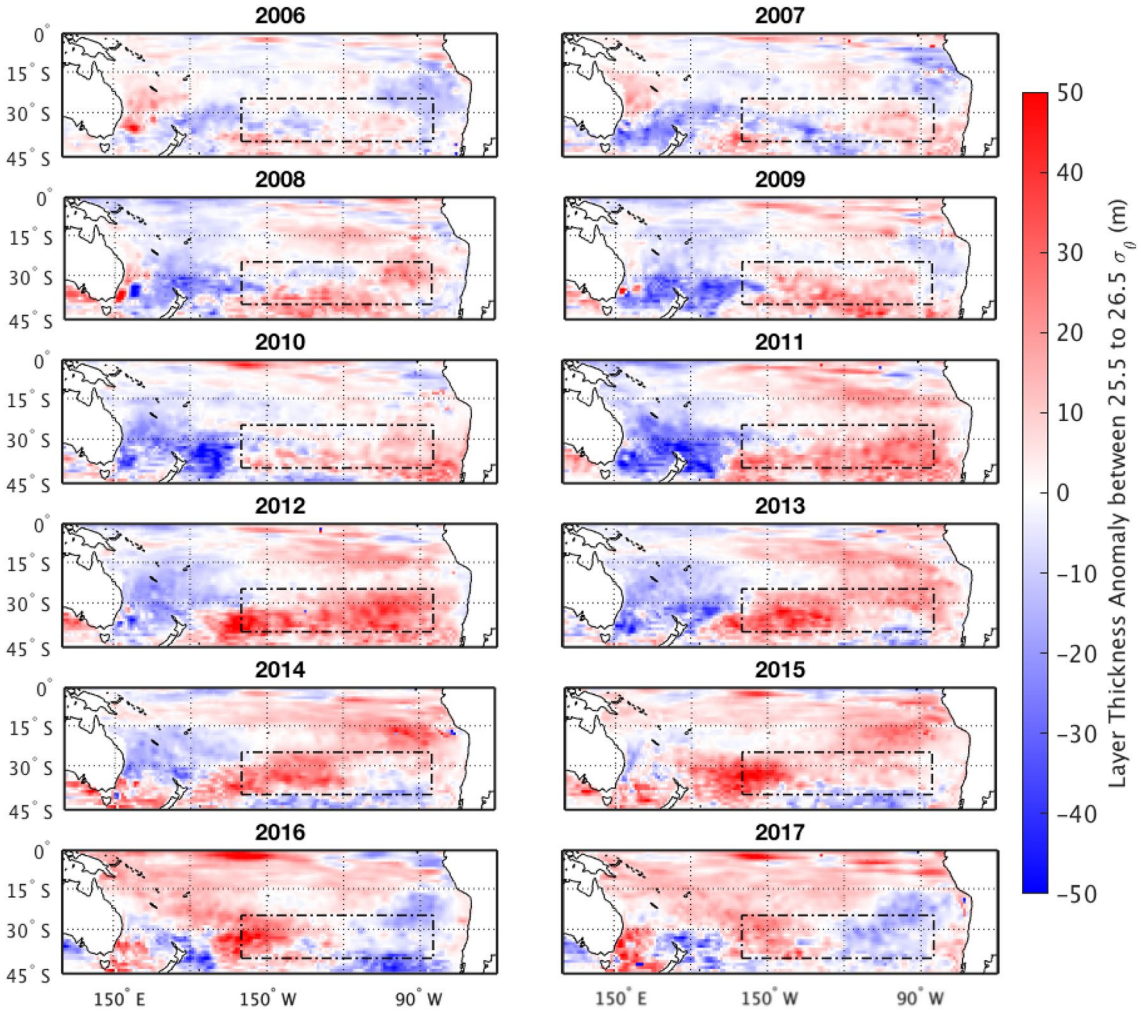

Fig. 1 Argo analysis of ventilated thermocline thickness. The difference in annual average thickness between the 25.5 and 26.5 potential density surfaces relative to 2004 is shown at yearly intervals (2006–2017) using Argo data. The development and westward/equatorward propagation of a positive thickness anomaly is evident in the Southern Hemisphere. The subduction region is indicated with a dashed line

the core where peak velocities increase by 20–30 cm/s, or roughly 20–25%. Focusing on depth integrated velocities greater than 80 cm/s, accounting for roughly half of the total eastward transport along the equator, EUC flow rates per unit width are 10–15% higher post-1999 than during the 1980s and 1990s.

4 Discussion

4.1 Thermocline structure: subtropical changes and equatorial circulation

The observed formation and propagation of thickness anomalies in the ventilated thermocline of the subtropical South Pacific is suggestive of a first-baroclinic mode Rossby wave (Figs. 1, 2). From 2011 to 2017, the anomaly appears to move westward along 35° S from around 115 to 160° W, traveling approximately 4000 km, in the opposite direction of the background flow driven by the easterly winds in the southern tropical Pacific. Although there is uncertainty as to defining the anomaly center and extent, this gives a phase speed on the order of 2–2.5 cm/s as evidenced in the Hovmoller diagram (Fig. 2). Theoretical predictions of the first-baroclinic mode Rossby wave speed in the non-dispersive, planetary-scale limit suggest a phase speed of 1.8 cm/s around 35° S in the southern subtropical Pacific (Chelton et al. 1998). Some of the discrepancy between theory and observations could be explained by the background shear flow in the gyre; Liu (1999) found that incorporating an eastward background flow increased westward propagation of baroclinic waves in a simplified, theoretical model.

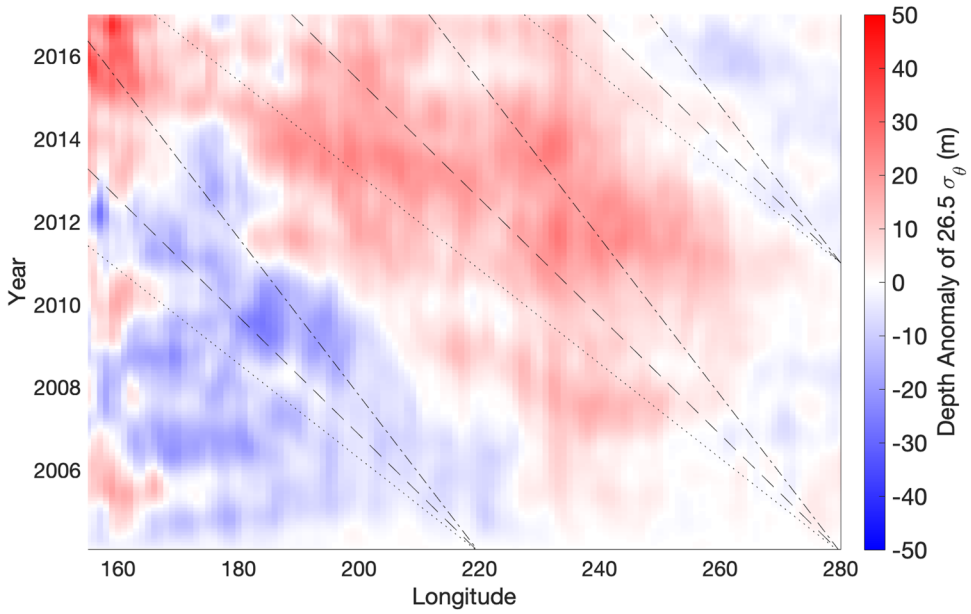

Fig. 2 Hovmoller diagram of depth anomalies of the base of the thermocline between 25 and 40° S. The thermocline depth anomaly of the 26.5 potential density surface relative to 2004 is shown from Argo data, averaged across 25–40°S and with a lowpass filter applied to remove the high-frequency, subannual signals. The development and propagation of a thermocline depression is evident in the later portion of the time period. Contour lines show westward propagation speeds of 1.5 cm/s, 2 cm/s, and 2.5 cm/s (dash-dotted, dashed, and dotted respectively). Figure S4 shows a similar diagram of thickness anomalies between the 25.5 and 26.5 potential density surfaces

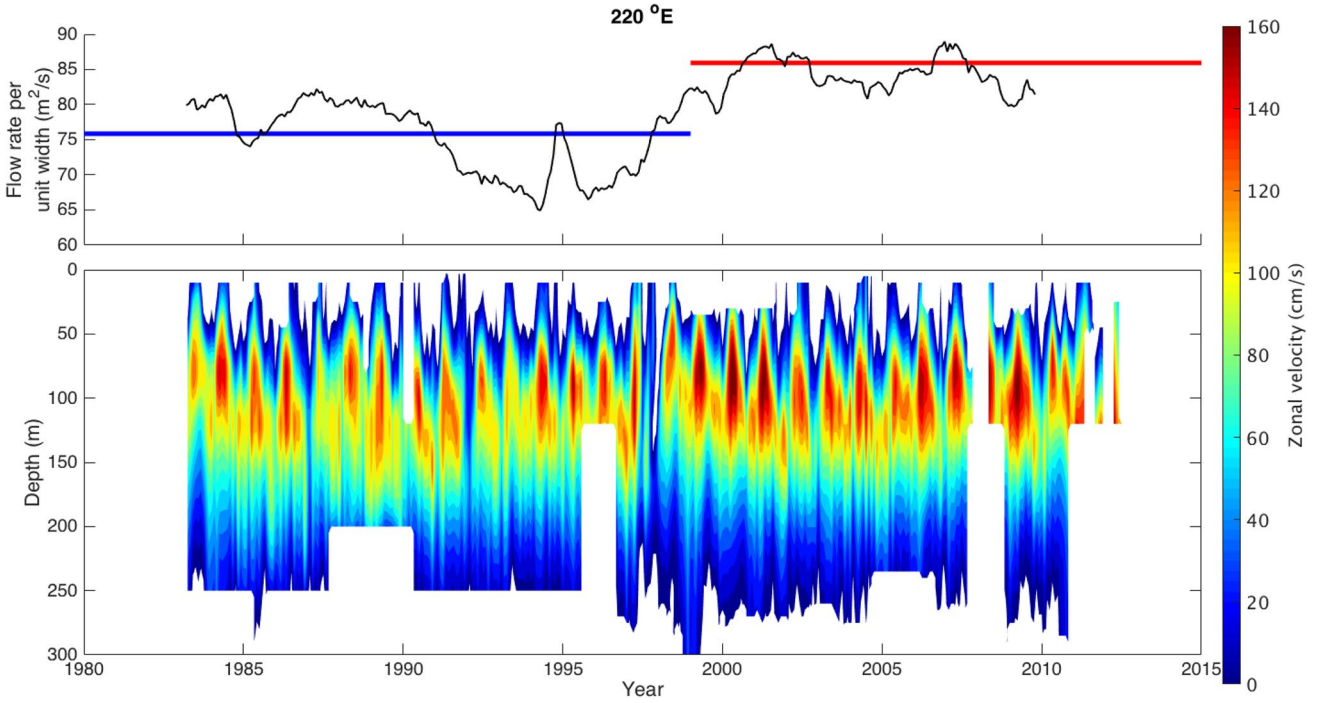

Fig. 3 Zonal velocity along the equator from the TAO buoy at 140° W, using both acoustic Doppler current profilers and current meter data. To focus on the EUC, only positive (eastward) zonal velocities are shown in the contour plot. An increase in current strength is evident post 1999. The line plot highlights this change, showing average flow rate per unit width above 80 cm/s before and after 1999, as well as the 5-years running mean (black). The record from the 110° W buoy shows a similar signal (Fig. S10), but the records from the other TAO buoys are not complete enough to perform this analysis

The lack of evidence for similar wave propagation in the North Pacific could stem from the weaker stratification in the lower layers of the ventilated thermocline as compared to the South Pacific (Kuntz and Schrag 2018). In both hemispheres, the upper layers of the ventilated thermocline extend to similar depths. However, in the North Pacific, the lower layers can extend up to 100 m deeper than in the South Pacific. This weaker stratification would amplify diapycnal mixing from internal waves,

increasing diffusivity and dissipation and inhibiting the propagation of planetary-scale baroclinic waves.

The baroclinic wave we observe in the South Pacific may be generated by wind stress anomalies in the South Pacific. During 2010 and 2011, when the baroclinic wave formed in the South Pacific due to a deepening of the lower layers of the ventilated thermocline, wind stress anomalies in this region reflected increased wind stress curl (figure S6, S7). By increasing Ekman pumping, this could be driving the wave formation. Variations in surface heat flux could also contribute to the observed deepening of the ventilated thermocline and deserves further investigation. However, given that for periods of the year these isopycnal layers are isolated from the surface in the South Pacific, it is unlike that would explain the entire signal.

These wind anomalies may be forced by the tropics. Previous work has already outlined a robust link between tropical heating anomalies and pressure anomalies in the South Pacific. In both observations and modeling, Trenberth et al. (2014) illustrated how tropical heating anomalies generate atmospheric Rossby waves. These Rossby waves propagate to the Eastern South Pacific, particularly in southern hemisphere winter, altering sea level pressure and subsequently surface winds. Trenberth et al. (2014) linked positive (negative) heating anomalies in the tropics with reduced (increased) wind stress curl in the region where we observe enhanced wind stress curl and the development of the baroclinic wave over 2010 and 2011. Additional modeling work by Luo et al. (2003) suggested these tropical-subtropical Rossby wave teleconnections could generate subtropical thermocline thickness anomalies and potentially contributing to tropical decadal variability. Our results provide additional observational support for such subsurface density changes.

How could such changes in off-equatorial thermocline structure affect circulation? Conceptual models of the thermocline predict that changes in the off-equatorial thermocline structure should modify streamline paths and subsequently equatorial circulation (Luyten et al. 1983; Pedlosky 1987; Huang and Pedlosky 1999, 2000). Specifically, Jin (2001), suggested that such off-equatorial changes can modify the depth of the equatorial thermocline. Changes in the equatorial thermocline can impact the EUC velocity by modulating the pressure head (static pressure from the depth of a thermocline layer) between the western and eastern equatorial Pacific through coupled, local ocean–atmosphere interactions. Once the baroclinic wave we have identified in the South Pacific reaches the western boundary, it should become a Kelvin wave that eventually deepens the equatorial thermocline, preferentially elevating temperatures in the eastern equatorial Pacific compared to the western equatorial Pacific. This would decrease the east–west SST gradient, reduce surface winds and diminish the equatorial pressure head. Subsequently, the EUC flow rate would decline to reach a new, lower steady-state flow. Given the large length-scale and slow propagation speed of the planetary-scale baroclinic wave, we expect that these equatorial changes should be more persistent and have a longer timescale than ENSO variability.

Model simulations support the predictions from simple theory. CMIP5 models with low vertical resolution between 150 and 400 m (vertical spacing between grid points is typically between 20 and 100 m) show little variability in the EUC and struggle to capture tropical Pacific variability (Roberts et al. 2009; Karnauskas et al. 2011; Yang et al. 2014). By increasing vertical resolution in the upper 400–10 m, the model shows a regular oscillation in the EUC velocity, coincident with the model ENSO with a period of roughly 4–5 years (Fig. 4a). We tested the impact of a subtropical thickness anomaly on the tropics by imposing and maintaining a depression of the 26.5 σ_θ surface by roughly 100 m in the subtropical South Pacific (30–40° S, 135° E–150° W), indicative of the observed anomaly in Argo. We also perform the same experiment, but with a shoaling of the subtropical thermocline. After a 5-years adjustment period, the thermocline's pressure head between the western and eastern equatorial Pacific responds to the subtropical anomaly. In the shoaling case, the pressure head rises, accelerating the EUC, and lowers Nino3.4 temperatures (Fig. 4b), as predicted from theory (Pedlosky 1987). The reverse happens for the depression of the subtropical thermocline (Fig. 4c), although the response is muted relative to the control simulation. Given that the model data were saved as monthly output, resolving the propagation of the coastal Kelvin wave in time is challenging as it should only take a few months to propagate from the mid-latitude to the equator. A Hovmoller diagram shows some evidence of coast wave propagation for the mid-latitude deepening and shoaling experiments (Fig. S9); however additional modeling efforts with higher temporal resolution of data output are a necessary next step to further clarify coastal Kelvin wave propagation.

The mid-latitude perturbations modify the equatorial isopycnal structure, particularly in the lower layers of the EUC, as shown in Fig. 5. In the shoaling experiment, the 26.5 σ_θ surface rises over the simulation at 140° W, suggestive of a wave communicating the mid-latitude signal. The change in the western Pacific is not as dramatic (Fig. S11), indicating that this asymmetric response increases the equatorial pressure head between the eastern and western Pacific, accelerating the EUC. Hovmoller diagrams of thermocline depth and thickness along the equator support the wave-like signal as well as the asymmetric equatorial response (Fig. S12 and S13). Introducing a deepening of the thermocline just off the equator (5–10° S, 130° E–150° W) clearly highlights the equatorial response. In contrast to the mid-latitude

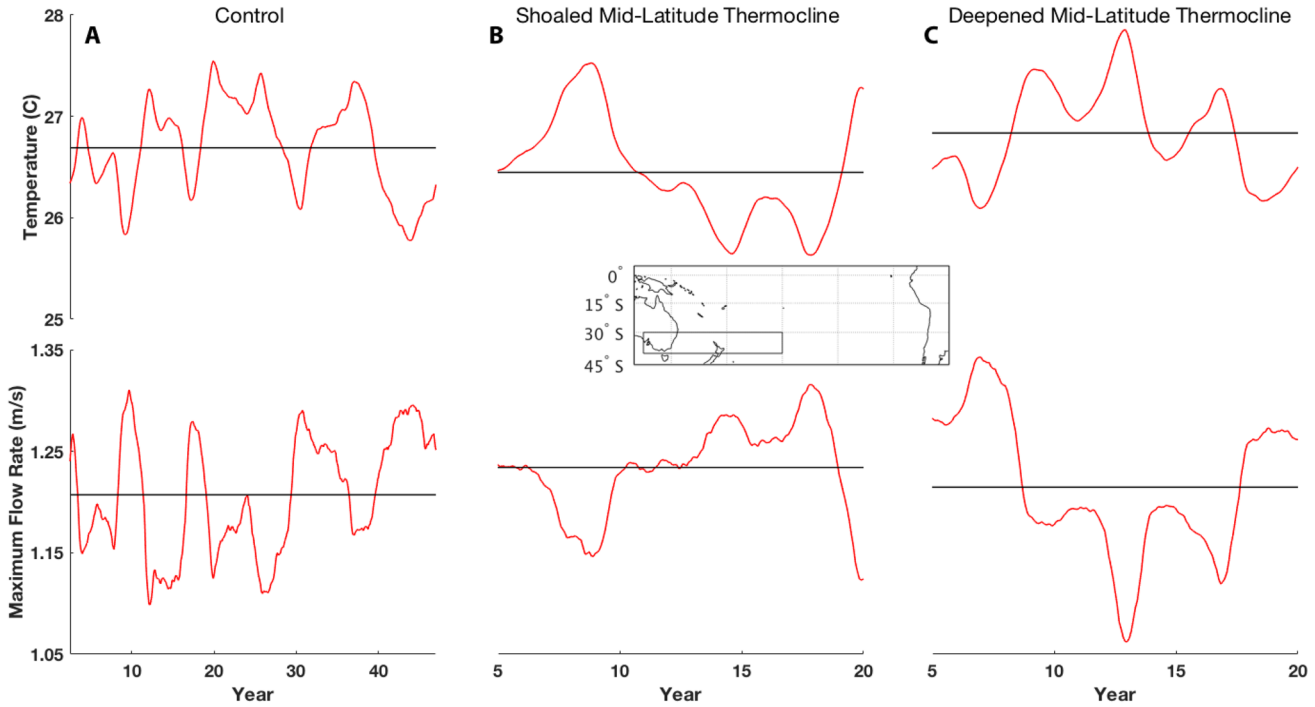

Fig. 4 Simulated relations between EUC flow rate, and Nino 3.4 temperature in a control simulation (**a**) when a shoaling (**b**) and when a depression of the thermocline is maintained in the subtropical South Pacific (30–40° S, 135° E−150° W) (**c**). The five-year running mean of Nino 3.4 temperature (top) and peak EUC velocity (bottom) is shown in red, while the simulation mean, after a 5-year adjustment period, is shown in black. Overlain on top of panel **b/c** is a map showing the region where the perturbation is applied. With a two-year running mean, Nino3.4 temperature and EUC strength have a correlation of −0.95

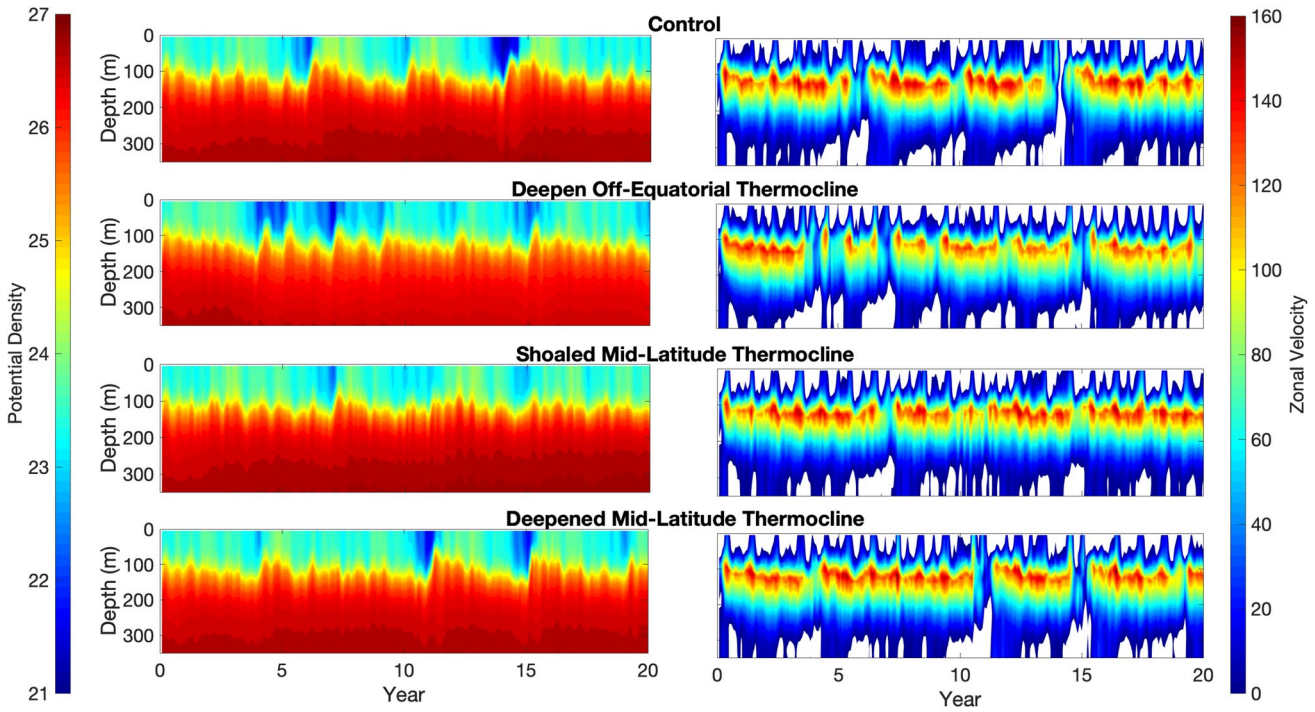

Fig. 5 Isopycnal structure (left) and zonal velocity (right) along the equator at 140° W in response to a perturbation that is maintained in the off-equatorial thermocline as well as a control simulation (top). Cases are shown for a depression of the off-equatorial thermocline (5–10° S, 130° E–150° W) (second), as well as a shoaling (third) and depression (bottom) of the subtropical South Pacific thermocline (30–40° S, 135° E–150° W)

shoaling experiment, the off-equatorial deepening depresses isopycnals in the lower layers of the ventilated thermocline at 140° W. This adjustment is sustained, with a persistent reduction of the equatorial pressure head and coincident with the maintained deceleration of the EUC. The depression of the mid-latitude thermocline does not show as strong of a response along the equator in isopycnal structure or EUC strength. Across the experiments with mid-latitude perturbations, the amplitude of the variability is roughly comparable to the control; however, the frequency of the variability has shifted. The frequency shift suggests sustained effects of thermocline modulation, but the similarity in signal amplitude complicates isolating the influence of subtropical thermocline shoaling and deepening. Future experiments could be performed to help isolate these effects—particularly varying the magnitude and distance from the equator of the perturbation could help elucidate signal attenuation. Given that the accuracy of EUC and equatorial simulation varies across climate models (Karnauskas et al. 2011; Kuntz and Schrag 2020), exploring the influence of model parameterizations on the influence of subtropical thermocline shoaling and deepening is another pathway for future work. Experiments on a suite of models with various resolutions and diffusivity parameterizations would clarify the sensitivity of the proposed mechanism to modeling choices.

The strength of the EUC is negatively correlated with Nino3.4 temperatures in both models and observations. At low frequencies, higher EUC speeds correspond with lower temperatures in the Nino3.4 region. This relationship holds at higher frequencies as well, although the relationship is non-linear; in the control simulation, monthly temperatures in the Nino3.4 region show more sensitivity to the changes in EUC speeds at the highest flow rates (Fig. 6). This asymmetric response could explain the greater sensitivity of the model simulation to a shoaling of the mid-latitude thermocline in the south Pacific, as opposed to a depression. Accelerating the EUC generates a stronger temperature response as compared to decelerating it. This relationship supports the hypothesis that the thermocline thickness anomaly that we observe in the south Pacific will ultimately decelerate the EUC and increase SSTs in the eastern equatorial Pacific as it reaches the equator.

In response to the thermocline perturbation, the IPO index also shifts towards a positive phase in the case of deepening and a negative phase in the case of shoaling (Fig. 7). Although the IPO index has no net positive or negative signal over the control simulation, after a 5-years adjustment period, the IPO index in the perturbation experiment has a mean value near 0.15 and −0.15 for the deepened and shoaled case, respectively. The PDO index also shows a similar response to the perturbation (Fig. S14). This suggests the possibility that subtropical changes in the southern subtropics and the subsequent changes in EUC strength can contribute to decadal variability not only in the tropics but also throughout the Pacific. As with the response of the SST and EUC speed, the magnitude of IPO signals in response to the perturbation are similar to the control, convoluting the strength of the influence of southern subtropical changes and subsequent EUC responses on decadal variability. There is still additional variability in both the IPO and PDO indices when the subtropical thermocline is perturbed, highlighting the role of many different sources of decadal variability in the Pacific in addition to EUC variability.

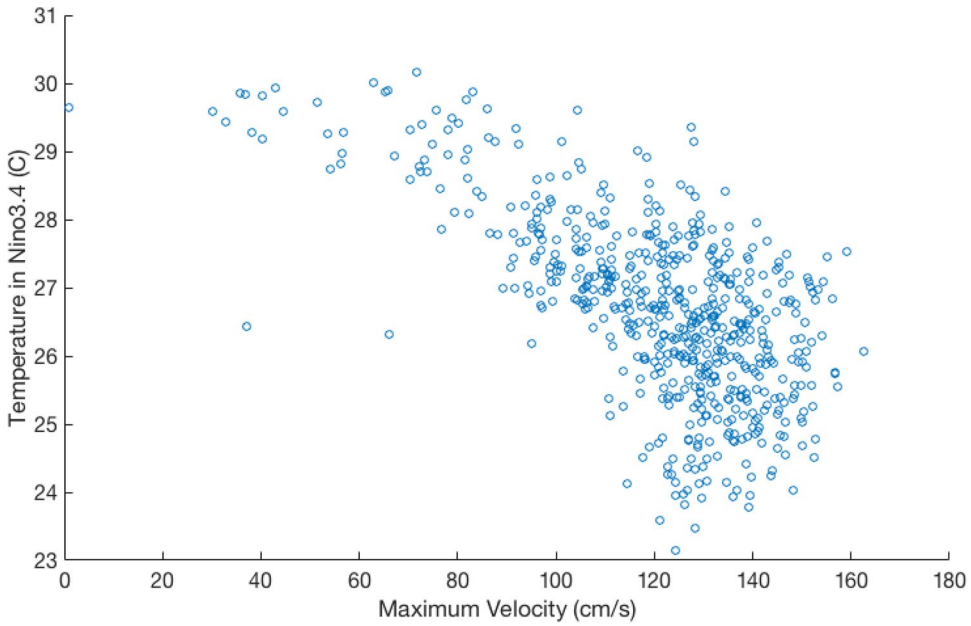

Fig. 6 Monthly maximum EUC velocities and Nino3.4 temperatures from a control simulation. There is no lag between the velocities and temperatures, although the general shape of the scatter plot is insensitive to lags up to a few months

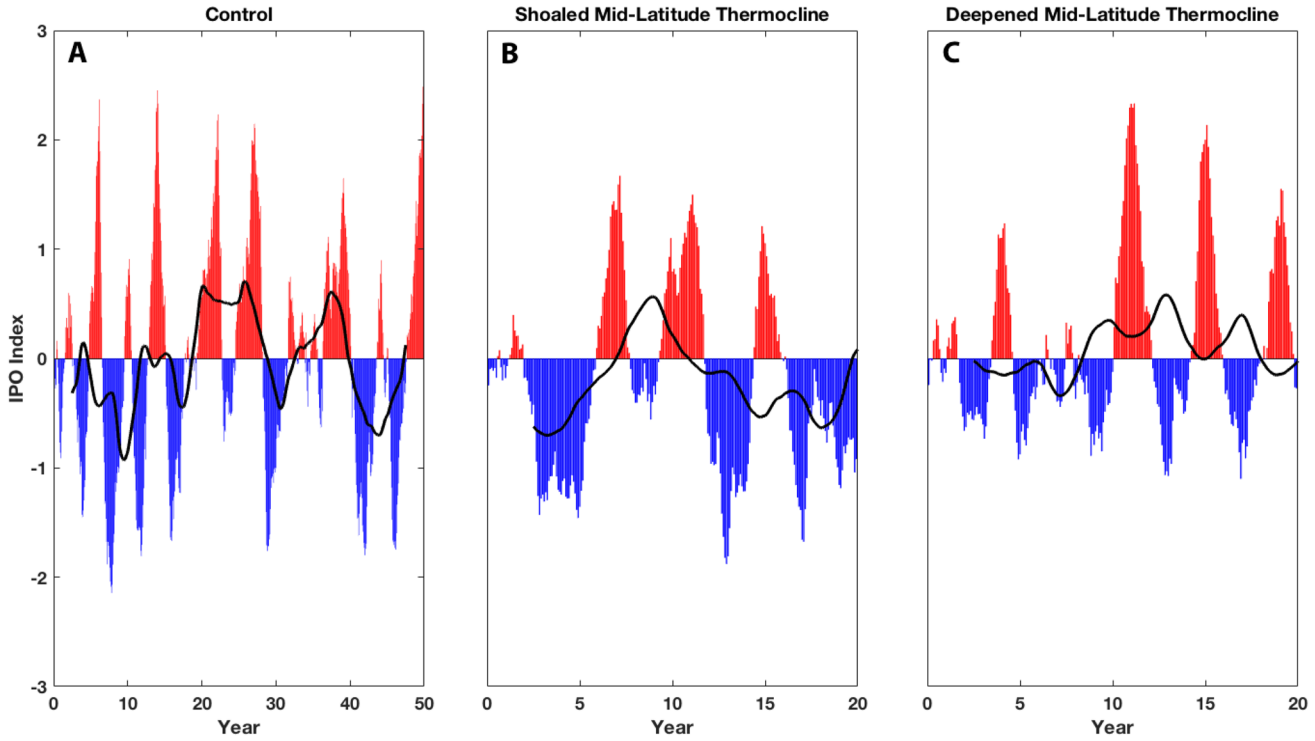

Fig. 7 IPO index from 50 years of a control simulation (**a**) and when a shoaling (**b**) and deepening (**c**) of the thermocline is maintained in the subtropical South Pacific (40° –30° S, 135° E–150° W). The red and blue bars indicate the monthly IPO index (for positive and negative values respectively), while the black line is the 5-years running mean

Do observations support such changes in EUC transport and Pacific variability? The baroclinic wave that we observe in the South Pacific in the Argo data has not yet reached the equator. We would expect it to depress the equatorial thermocline, ultimately slowing the EUC and shifting the Pacific to a warm state, but we cannot yet test this predicted tropical response. However, we can look at past changes in the state of the Pacific to see if they align with EUC variability as expected. Around 2000, when the PDO transitioned from a positive to a negative phase, subsurface velocity measurements from the TAO buoy array show acceleration in the EUC flow (Fig. 3). Because of the coupled nature of the equatorial Pacific, it is difficult to rule out the possibility of simultaneous changes in winds and external surface forcings that could contribute to this EUC acceleration, but we note that the observed decadal shift aligns with the change we would expect from the arrival of a subtropical upwelling baroclinic wave. As the TAO buoys only measure velocity at point locations, it is possible that the apparent strengthening of the EUC is due to a meridional shift or narrowing of the current. However, the consistency of the pattern between locations is intriguing. Other studies, which have noted increases in meridional mass flux over this same period (McPhaden and Zhang 2002, 2004; Zhang and McPhaden 2006; Amaya et al. 2015), also lend strength to the interpretation of the signal as an increase in EUC strength driven by the subtropics.

The TAO array only covers the most recent PDO phase transition. However, evidence from coral radiocarbon records suggests a similar shift in EUC strength aligned with the phase transition in 1976/1977. Guilderson and Schrag (1998) noticed an abrupt shift in both upwelling temperatures in the eastern Pacific as well as radiocarbon values in Galapagos coral in 1976, suggestive of changes in the thermocline's vertical density structure. Guilderson and Schrag (1998) speculated this thermocline variability stemmed from a shift in the relative contribution of northern and southern hemisphere source waters. A simpler explanation for this is a reduction in the velocity of the EUC that reduces entrainment of deeper, low radiocarbon content water along the path of EUC transport. Thus, the radiocarbon data could be consistent with a reduction in EUC velocity, analogous to what we anticipate will happen when the baroclinic wave we currently observe in the South Pacific reaches the equator.

4.2 A mechanism of Pacific variability

The cumulative evidence from observations of the propagation of changes in thermocline structure along with changes in EUC velocity coincident with decadal variability in the

Pacific, coupled with theory and model simulations, build up the work of Lysne et al (1997) and Jin (2001) to support a hypothesis for a mode of decadal variability in the tropical Pacific. The timescale of this mode is dictated by the baroclinic adjustment of the ventilated thermocline. From an initial state (such as the one currently observed) with a negative phase of the PDO and high EUC flow rates, anomalously strong wind stress curl (as noted from reanalysis and model simulations in Luo et al. 2003 and Trenberth et al. 2014) enhances Ekman pumping in the subtropics, depressing the deeper layers of the ventilated thermocline and increasing isopycnal layer thickness in the south-eastern Pacific. This generates planetary-scale baroclinic waves, which propagate westward across the basin over 1–2 decades. Upon reaching the western boundary, the baroclinic waves become Kelvin waves, rapidly propagating to the equatorial Pacific and adjusting the thermocline depth, as noted in theory by Jin (2001). Changes in the thermocline disproportionately reflect onto increased temperatures in the eastern equatorial Pacific, decreasing the east–west SST gradient and surface winds. Reduced winds decrease equatorial pressure head, weakening EUC transport, further elevating temperatures in the eastern equatorial Pacific and contributing to a shift of the IPO and PDO to a positive phase. Although this hypothesis proposes a mechanism for the tropical component of Pacific variability, it does not preclude other factors from contributing to subtropical Pacific variability, including changes in the Aleutian low, Kuroshio-Oyashio system, and ocean memory (Newman et al. 2016).

An atmospheric bridge between the tropics and subtropics would allow this cycle to be self-sustaining. PDO-related anomalies in equatorial Pacific SST modulate sea level pressure (SLP) in the South Pacific, and associated wind stress curl through atmospheric Rossby waves (Luo et al. 2003; Trenberth et al. 2014). In the negative (cold) PDO phase, higher SLP and elevated wind stress curl leads to enhanced Ekman pumping, depressing the thermocline and generating positive thickness anomalies that propagate as baroclinic waves. In the positive (warm) PDO phase, lower SLP and reduced wind stress leads to decreased Ekman pumping, elevating the thermocline and generating upwelling baroclinic waves with negative thickness anomalies.

This proposed mechanism is similar to the delayed oscillator theory for ENSO (Battisti 1988; Suarez and Schopf 1988; Battisti and Hirst 1989), but is driven by baroclinic and Kelvin waves that originate in the subtropics, rather than being confined to the tropics. Previous work by Galanti and Tziperman (2003) suggested how subtropical baroclinic waves could modify the equatorial Pacific, highlighting waves advected by the gyre circulation. In contrast, here we observe and focus on westward propagating planetary-scale first-baroclinic mode waves. These waves are not impacted by the gyre circulation and should propagate directly westward (Liu 1999) until becoming Kelvin waves at the ocean boundary. This mechanism is more indicative of the ideas proposed by Jin (2001) and Luo et al (2003), with subtropical modulation of the tropics through thermocline thickness anomalies. Our hypothesis, however, explicitly shows the wave propagation and equatorial circulation anomalies responsible for this oceanic bridge, providing observational support for the idea. In a notable distinction from Jin (2001), the observed Rossby wave originates at a higher latitude. Jin's idea did not exclude this possibility, but the drivers behind the wave origin location are worth further investigation. Unlike the delayed oscillator theory, which is stochastically forced, the mechanism we propose could oscillate and may be self-sustaining due to atmospheric teleconnections, although there may be some role for stochastic forcing as well. The propagation time for the subtropical baroclinic Rossby wave—on the order of 10–15 years—increases the timescale of variability compared to the delayed oscillator. The propagation timescale is not directly equivalent to the timescale of the cycle; just as the delayed oscillator wave propagation timescale of 6–8 months leads to a 2–7-years cycle, this mechanism's baroclinic timescale could lead to a multi-decadal cycle of 50–60 years assuming a similar ratio of wave propagation to oscillation timescales.

How could models be improved to allow them to simulate the internal mode of decadal variability we describe here? Atmosphere models are able to recreate the Rossby wave trains between the topics and subtropics that drive SLP and wind stress anomalies (Trenberth et al. 2014). However, little emphasis has been placed on understanding the required vertical resolution in ocean models to capture the horizontal flows from baroclinic waves. Stewart et al (2017) suggest that a minimum of 50 well-placed vertical levels are necessary to resolve first-mode baroclinic waves. Our simulations use 70 vertical levels, with 10 m resolution in the top 400 m, yet not all current models have well-placed vertical grids. This metric does not consider how wave propagation is impacted by parameterized diffusivity, which has been shown to impact the base state of the thermocline and EUC in model simulations (Charney and Spiegel 1971; Gregg 1987), and could overdamp baroclinic disturbances (Marchal 2009). Enhanced vertical and horizontal resolution has been shown to increase the accuracy of EUC simulations (Roberts et al. 2009; Karnauskas et al. 2011), and might allow models to better simulate the proposed mechanism. Isopycnal models may improve some of the challenges of vertical grid selection, although some of the isopycnal models that are part of the CMIP5 ensemble do not capture the key features of equatorial dynamics (Bellenger et al. 2014). The horizontal resolution of the CESM model used here resolves the EUC and equatorial Kelvin waves, but it does not resolve mesoscale eddies or western boundary currents. Models with enhanced resolution capable of capturing the Rossby radius in the mid-latitudes resolve both of these

and have shown improvements in ocean heat transport (Hewitt et al. 2016). Given the importance of these features, further modeling work with increased horizontal resolution or high-resolution regional ocean models could help elucidate the fidelity and impacts of the proposed mechanism.

If our hypothesis of subtropical thermocline anomalies modulating equatorial dynamics is correct, then adjustment of the circulation to the thermocline depression will drive a reduction in EUC strength. Reduced EUC speed will contribute to changes in the state of the Pacific, helping drive the reversal of the phase of the PDO. Based on the observed phase speed of the baroclinic wave and the 3-year time delay of the model's response to an imposed depression in the off-equatorial thermocline, we anticipate this phase change should happen between 2020 and 2025.

5 Conclusion

Observations, model, and theory support a new mechanism for decadal variability in the tropical Pacific. On timescales set by wave adjustment, anomalies in the structure of the ventilated thermocline develop and propagate as baroclinic and Kelvin waves from the southeast Pacific to the equator, where, through coupled ocean–atmosphere interactions, they modulate the strength of the EUC. Observations from the TAO array show evidence for such decadal variability of EUC strength, with an amplification of flows coincident with the transition from a positive to negative phase of the PDO. The hypothesized mechanism of decadal EUC adjustment could explain some of the variability in the eastern Pacific and PDO. An atmospheric teleconnection between the equatorial and subtropical Pacific could amplify and periodically reverses the thermocline anomaly. Argo data reveal the development and propagation of such a thermocline anomaly as a baroclinic wave. Over the next decade, this wave should reach the equator and decelerate the EUC. If correct, the suggested mechanism indicates that subtropical-tropical pathways in the South Pacific can contribute to internal, decadal variability in the ocean.

Acknowledgments We thank Greg Johnson for assisting with access to TAO data. We thank Mark Cane for advice and inspiration. This material is based upon work supported by a National Science Foundation Graduate Research Fellowship (Grant Number DGE1144152) to LBK and a Star Family Challenge Grant to DPS. Data from the Tropical Atmosphere Ocean Project came from the TAO Project Office of NOAA/PMEL. This study was conducted using E.U. Copernicus Marine Services Information.

References

Amaya DJ, Xie S-P, Miller AJ, McPhaden MJ (2015) Seasonality of tropical Pacific decadal trends associated with the 21st century global warming hiatus. J Geophys Res Oceans 120:6782–6798. https://doi.org/10.1002/2015JC010906

Barsugli JJ, Battisti DS (1998) The basic effects of atmosphere-ocean thermal coupling on midlatitude variability. J Atmos Sci 55:477–493. https://doi.org/10.1175/1520-0469(1998)055%3c0477:TBEOAO%3e2.0.CO;2

Battisti DS (1988) Dynamics and thermodynamics of a warming event in a coupled tropical atmosphere-ocean model. J Atmos Sci 45:2889–2919. https://doi.org/10.1175/1520-0469(1988)045%3c2889:DATOAW%3e2.0.CO;2

Battisti DS, Hirst AC (1989) Interannual variability in a tropical atmosphere-ocean model: influence of the basic state ocean geometry, and nonlinearity. J Atmos Sci 46:1687–1712. https://doi.org/10.1175/1520-0469(1989)046%3c1687:IVIATA%3e2.0.CO;2

Bellenger H, Guilyardi E, Leloup J, Lengaigne M, Vialard J (2014) ENSO representation in climate models: from CMIP3 to CMIP5. Clim Dyn 42:1999–2018. https://doi.org/10.1007/s00382-013-1783-z

Bratcher AJ, Giese BS (2002) Tropical Pacific decadal variability and global warming. Geophys Res Lett 29:1918. https://doi.org/10.1029/2002GL015191

Broecker WS, Peng T-H, Ostlund G, Stuiver M (1985) The distribution of bomb radiocarbon in the ocean. J Geophys Res 90:6953–6970. https://doi.org/10.1029/JC090iC04p06953

Broecker WS, Sutherland S, Smethie W, Peng T-H, Ostlund G (1995) Oceanic radiocarbon: Separation of the natural and bomb components. Global Biogeochem Cycles 9:263–288. https://doi.org/10.1029/95GB00208

Charney JG, Spiegel SL (1971) Structure of wind-driven equatorial currents in homogeneous oceans. J Phys Oceanogr 1:149–160. https://doi.org/10.1175/1520-0485(1971)001%3C0149:SOWDEC%3E2.0.CO;2

Chelton DB, Schlax MG (1996) Global observations of oceanic Rossby waves. Science 272:234–238. https://doi.org/10.1126/science.272.5259.234

Chelton DB, DeSzoeke RA, Schlax MG (1998) Geographic variability of the first baroclinic rossby radius of deformation. J Phys Oceanogr 28:433–460. https://doi.org/10.1175/1520-0485(1998)028%3c0433:GVOTFB%3e2.0.CO;2

Chelton DB, Schlax MG, Samelson RM, de Szoeke RA (2007) Global observations of large oceanic eddies. Geophys Res Lett 34:15606. https://doi.org/10.1029/2007GL030812

Dee DP et al (2011) The ERA-Interim renanalysis: configuration and performance of data assimilation system. Q J Roy Meteor Soc 137:553–597. https://doi.org/10.1002/qj.828

Druffel ERM (1987) Bomb radiocarbon in the Pacific: annual and seasonal timescale variations. J Mar Res 45:667–698. https://doi.org/10.1357/002224087788326876

Fine RA, Peterson WH, Ostlund HG (1987) The penetration of tritium into the tropical pacific. J Phys Oceanogr 17:553–564. https://doi.org/10.1175/1520-0485(1987)017<0553:TPOTIT>2.0.CO;2

Galanti E, Tziperman E (2003) A midlatitude-ENSO teleconnection mechanism via baroclinically unstable long rossby waves. J Phys Oceanogr 33:1877–1888. https://doi.org/10.1175/1520-0485(2003)033%3c1877:AMTMVB%3e2.0.CO;2

Giese BS, Urizar SC, Fučkar NS (2002) Southern Hemisphere origins of the 1976 climate shift. Geophys Res Lett 29:1014. https://doi.org/10.1029/2001GL013268

Godfrey JS (1975) On ocean spindown I: a linear experiment. J Phys Oceanogr 5:399–409. https://doi.org/10.1175/1520-0485(1975)005%3c0399:OOSIAL%3e2.0.CO;2

Gregg MC (1987) Diapycnal mixing in the thermocline: a review. J Geophys Res 92:5249–5286. https://doi.org/10.1029/JC092iC05p05249

Gu D, Philander SGH (1997) Interdecadal climate fluctuations that depend on exchanges between the tropics and extratropics. Science 275:805–807. https://doi.org/10.1126/science.275.5301.805

Guilderson TP, Schrag DP (1998) Abrupt shift in subsurface temperatures in the tropical Pacific associated with changes in El Nino. Science 281:240–243. https://doi.org/10.1126/science.281.5374.240

Hazeleger W, Visbeck M, Cane M, Karspeck A, Naik N (2001) Decadal upper ocean temperature variability in the tropical Pacific. J Geophys Res 106:8971–8988. https://doi.org/10.1029/2000JC000536

Hewitt HT et al (2016) The impact of resolving the Rossby radius at mid-latitudes in the ocean: results from a high-resolution version of the Met Office GC2 coupled model. Geosci Model Dev 9:3655–3670. https://doi.org/10.5194/gmd-9-3655-2016

Huang RX, Pedlosky J (1999) Climate variability inferred from a layered model of the ventilated thermocline. J Phys Oceanogr 29:779–790. https://doi.org/10.1175/1520-0485(1999)029%3c0779:CVIFAL%3e2.0.CO;2

Huang RX, Pedlosky J (2000) Climate variability of the equatorial thermocline inferred from a two-moving-layer model of the ventilated thermocline. J Phys Oceanogr 30:2610–2626. https://doi.org/10.1175/1520-0485(2000)030%3c2610:CVOTET%3e2.0.CO;2

Hurrell JW et al (2013) The community earth system model: a framework for collaborative research. Bull Amer Meteor 94:1339–1360. https://doi.org/10.1175/BAMS-D-12-00121.1

Jin F-F (2001) Low-frequency modes of tropical ocean dynamics. J Clim 14:3874–3881. https://doi.org/10.1175/1520-0442(2001)014%3c3874:LFMOTO%3e2.0.CO;2

Karnauskas KB, Johnson GC, Murtugudde R (2011) An equatorial ocean bottleneck in global climate models. J Clim 25:343–349. https://doi.org/10.1175/JCLI-D-11-00059.1

Kleeman R, McCreary JP, Klinger BA (1999) A mechanism for generating ENSO decadal variability. Geophys Res Lett 26:1743–1746. https://doi.org/10.1029/1999GL900352

Kolodziejczyk N, Gaillard F (2012) Observation of spiciness interannual variability in the Pacific pycnocline. J Geophys Res 117:C12018. https://doi.org/10.1029/2012JC008365

Kuntz LB, Schrag DP (2018) Hemispheric asymmetry in the ventilated thermocline of the tropical Pacific. J Clim 31:1281–1288. https://doi.org/10.1175/JCLI-D-17-0686.1

Kuntz LB, Schrag DP (2020) Representation of the equatorial undercurrent in CMIP5 models. J Phys Oceanogr. https://doi.org/10.1175/JPO-D-20-0007.1

Liu Z (1999) Planetary wave modes in the thermocline: non-Doppler-shift mode, advective mode and Green mode. Q J R Meteorol Soc 125:1315–1339. https://doi.org/10.1002/qj.1999.49712555611

Luo J-J, Masson S, Behera S, Delecluse P, Gualdi S, Navarra A, Yamagata T (2003) South Pacific origin of the decadal ENSO-like variation as simulated by a coupled GCM. Geophys Res Lett 30:2250. https://doi.org/10.1029/2003GL018649

Luyten JR, Pedlosky J, Strommel H (1983) The ventilated thermocline. J Phys Oceanogr 13:292–309. https://doi.org/10.1175/1520-0485(1983)013%3c0292:TVT%3e2.0.CO;2

Lysne J, Chang P, Giese B (1997) Impact of the extratropical Pacific on equatorial variability. Geophys Res Lett 24:2589–2592. https://doi.org/10.1029/97GL02751

Mantua NJ, Hare SR (2002) The Pacific decadal oscillation. J Oceanogr 58:35–44

Marchal O (2009) Extratropical rossby waves in the presence of buoyancy mixing. J Phys Oceanogr 39:2910–2925. https://doi.org/10.1175/2009JPO4139.1

McPhaden MJ, Zhang D (2002) Slowdown of the meridional overturning circulation in the upper Pacific Ocean. Nature 415:603–608. https://doi.org/10.1038/415603a

McPhaden MJ, Zhang D (2004) Pacific Ocean circulation rebounds. Geophys Res Lett 31:L18301. https://doi.org/10.1029/2004GL020727

Newman M, Coauthors, (2016) The Pacific Decadal oscillation, revisited. J Clim 29:4399–4427. https://doi.org/10.1175/JCLI-D-15-0508.1

Newman M, Compo GP, Alexander MA (2003) ENSO-forced variability of the Pacific Decadal Oscillation. J Clim 16:3853–3857. https://doi.org/10.1175/1520-0442(2003)016%3c3853:EVOTPD%3e2.0.CO;2

Ng MKF, Hsieh WW (1994) The equatorial Kelvin wave in finite difference models. J Geophys Res 99:14173–14185. https://doi.org/10.1029/94JC00473

Pedlosky J (1987) An inertial theory of the equatorial undercurrent. J Phys Oceanogr 17:1978–1985. https://doi.org/10.1175/1520-0485(1987)017%3c1978:AITOTE%3e2.0.CO;2

Roberts MJ et al (2009) Impact of resolution on the Tropical Pacific circulation in a matrix of coupled models. J Clim 22:2541–2556. https://doi.org/10.1175/2008JCLI2537.1

Rodgers KB, Cane MA, Naik NH, Schrag DP (1999) The role of the Indonesian Throughflow in equatorial Pacific thermocline ventilation. J Geophys Res 104:20551–20570. https://doi.org/10.1029/1998JC900094

Rodgers KB, Blanke B, Madec G, Aumont O, Ciais P, Dutay J-C (2003) Extratropical sources of Equatorial Pacific upwelling in an OGCM. Geophys. Res. Lett. 30:1084. https://doi.org/10.1029/2002GL016003

Roemmich D, Gilson J (2009) The 2004–2008 mean and annual cycle of temperature, salinity, and steric height in the global ocean from the Argo Program. Prog Oceanogr 82:81–100. https://doi.org/10.1016/j.pocean.2009.03.004

Roemmich, D., and J. Gilson (2018) Roemmich-Gilson Argo climatology. Scripps Institution of Oceanography. Subset used: January 2004–December 2017. http://sio-argo.ucsd.edu/RG_Climatology.html. **(Accessed 25 Apr 2018)**

Schneider N, Venzke S, Miller AJ, Pierce DW, Barnett TP, Deser C, Latif M (1999b) Pacific thermocline bridge revisited. Geophys Res Lett 26:1329–1332. https://doi.org/10.1029/1999GL900222

Schneider N, Miller AJ, Alexander MA, Deser C (1999a) Subduction of decadal North Pacific temperature anomalies: observations and dynamics. J Phys Oceanogr 29:1056–1070. https://doi.org/10.1175/1520-0485(1999)029,1056:SODNPT.2.0.CO;2

Stewart KD, McC A, Hogg SM, Griffies AP, Heerdegen ML, Ward PS, England MH (2017) Vertical resolution of baroclinic modes in global ocean models. Ocean Model 113:50–65. https://doi.org/10.1016/j.ocemod.2017.03.012

Suarez MJ, Schopf PS (1988) A delayed action oscillator for ENSO. J Atmos Sci 45:3283–3287. https://doi.org/10.1175/1520-0469(1988)045%3c3283:ADAOFE%3e2.0.CO;2

TAO Project Office (2000) Tropical atmosphere ocean/triangle trans-ocean buoy network. NOAA/PMEL. https://www.pmel.noaa.gov/tao/drupal/disdel/. **(Accessed 21 Jul 2016)**

Trenberth KE, Hurrell JW (1994) Decadal atmosphere-ocean variations in the Pacific. Clim Dyn 9:303–319

Trenberth KE, Fasullo JT, Branstator G, Phillips AS (2014) Seasonal aspects of the recent pause in surface warming. Nat Clim Change 4:911–916. https://doi.org/10.1038/nclimate2341

von Schuckmann K, Coauthors (2016) The Copernicus Marine Environment Monitoring Service ocean state report. J Oper Oceanogr 9:s235–s320. https://doi.org/10.1080/1755876X.2016.1273446

Yang C, Giese BS, Wu L (2014) Ocean dynamics and tropical Pacific climate change in ocean reanalyses and coupled climate models. J Geophys Res Oceans 119:7066–7077. https://doi.org/10.1002/2014JC009979

Zhang D, McPhaden MJ (2006) Decadal variability of the shallow Pacific meridional overturning circulation: relation to tropical sea surface temperatures in observations and climate change models. Ocean Model 15:250–273. https://doi.org/10.1016/j.ocemod.2005.12.005

Zhang X, McPhaden MJ (2010) Surface layer heat balance in the eastern equatorial Pacific ocean on interannual time scales: influence of local versus remote wind forcing. J Clim 23:4375–4394. https://doi.org/10.1175/2010JCLI3469.1